



Investigation on structural behavior of ring-stiffened composite offshore rubber hose under internal pressure



Qiang Gao^a, Peng Zhang^a, Menglan Duan^{a,b}, Xueqi Yang^a, Wenbin Shi^a, Chen An^{b,*}, Zhongli Li^c

^a Department of aeronautics and astronautics, Fudan University, Shanghai, China

^b Institute for Ocean Engineering, China University of Petroleum, Beijing, China

^c Hebei Jingxian Zebang Rubber Technology, Co., Ltd, Hengshui, China

ARTICLE INFO

Keywords:

Stiffened composite rubber hose
Single carcass
Stiffener
Rebar
Failure pressure

ABSTRACT

Ring-stiffened composite offshore rubber hose of single carcass is commonly used for offshore oil transfer. Common hose dimensions are length of 10.7 m and nominal diameter of 500 mm. The nominal burst pressure is 7.5 MPa, equal to five times rated working pressure of 1.5 MPa. The hose carcass is composite cylindrical tube made of rubber, reinforcing fiber cords and steel spiral stiffener that provides radial stiffness. In hose design, the burst pressure shall be determined to verify its pressure bearing capacity. In this paper, a nonlinear finite element hose model is created with commercial software ABAQUS and validated to predict its structural behavior under internal pressure. The large deformations, interactions between components and nonlinear material properties of hyperelastic rubber and fibers are considered. Stresses of stiffener, radial and axial deformation and load in reinforcement plies are obtained. A bulging phenomenon amid two stiffeners is found, which indicates the confine effect of stiffeners. Failure pressure is jointly determined by the strength limit of polymer cords and steel stiffener. The influence of different fibers and rubbers on hose pressure-deformation response are compared. The results demonstrate good accordance with requirement of specification. The finite element model can predict hose failure pressure and provide guidance for reliable hose design in practice.

1. Introduction

Offshore floating rubber hose of single carcass is used for oil transfer in offshore oil field, such as conveying crude oil from floating production storage and offloading (FPSO) to export tanker. The hose floats on sea surface by integrated floatation foam under working conditions. It is also widely used in single point moorings which are particularly suited to the handling of large tankers at offshore locations [1]. The composite rubber hose is manufactured with prescribed length due to the dimension limitation of vulcanizing tank. Northcutt presents an overview of composite hose in offshore development [2]. It is an economical and feasible solution for hydrocarbon transfer.

The hose construction is depicted in Fig. 1 and Fig. 2. The geometric parameters are listed in Table 1. It is a composite structure with complex cross section. All of its structural parts are bonded together by rubber vulcanization. Interlayer bonding will prevent gaps and relative slip between layers. The hose has a typical single carcass composed of rubber, rubberized cord fabric (or named cord-rubber reinforcement) plies and a spiral stiffener. The steel end fitting comprises the flange, annular ribs and nipple. The annular ribs assist the binding steel wires

to anchor various structural layers on the nipple. The nipple can transmit axial loads and bending moments from flange to hose body. The inner lining is made of oil inert nitrile butadiene rubber. The lining provides sealing capacity and protects the reinforcement layers from oil corrosion. The reinforcement plies are composed of cords embedded in elastomeric matrix, namely rubberized cord fabric, as shown in Fig. 3. The fabric is made of nylon or polyester cord, which includes numerous filaments. They are arranged at crossed $\pm\theta$ angles with respect to longitudinal hose axis, withstanding internal pressure and axial load. The angle-ply reinforcement plies are designed to achieve maximum strength and flexibility with minimum axial elongation.

In this paper, the nominal hose bore diameter is 500 mm and the rated working pressure is 1.5 MPa. As shown in Fig. 4, the steel helix wire is continuous without intermediate welding, embedded in the rubber between two reinforcement layers. The wire diameter is 12 mm with a pitch of 50 mm. The helix is wound at an angle nearly close to 90° relative to hose longitudinal axis. It increases radial stiffness of cross section and prevents ovalisation of hose section due to vacuum or bending. The floatation jacket is closed-cell foam, giving buoyancy over the entire hose length. Finally, a reinforced elastomeric layer with

* Corresponding author.

E-mail address: anchen@cup.edu.cn (C. An).

<https://doi.org/10.1016/j.apor.2018.07.007>

Received 4 April 2018; Received in revised form 6 June 2018; Accepted 13 July 2018

0141-1187/© 2018 Elsevier Ltd. All rights reserved.

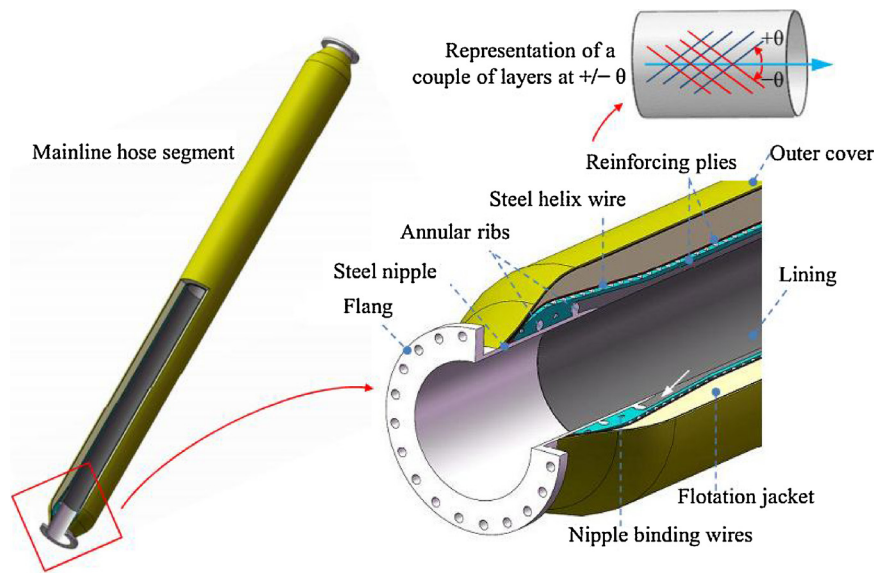


Fig. 1. Components of stiffened composite hose.

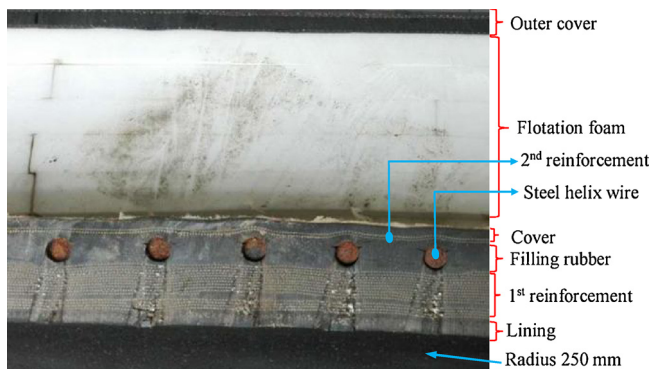


Fig. 2. Layout of composite hose body (longitudinal profile).

Table 1
Geometric parameters of the analyzed model.

Parameter	Value	Parameter	Value
Nominal inner radius (mm) r_0	250	Mean helix radius (mm)	284.6
Outer radius (mm)	294.4	Helix wire diameter (mm)	12
Number of plies in 1 st and 2 nd reinforcement layer	14; 2	Pitch of helix (mm)	50
Winding angle φ ($^\circ$) of reinforcement layers	+45 $^\circ$ /-45 $^\circ$	Length of the model (mm)	150

gridding cloth named cover, is laid on the floatation, making hose resistant to abrasion, weathering and sea water.

In offshore hose industry, engineers usually refer to two standards for hose structural design and verification, i.e. OCIMF 2009 [3] and API 17 K 2010 [4]. OCIMF 2009 provides technical requirements to ensure the satisfactory performance of elastomer reinforced, smooth bore, oil suction and discharge hose commonly used at offshore moorings. The performances of various materials like rubber, cords and steel are specified. It offers procedures and acceptance criteria of kinds of prototype tests, like burst, torsion and tensile test. API 17 K applies to a wider range of bonded flexible pipe than OCIMF 2009. It gives requirements for the design procedure, material selection, manufacture, testing of bonded flexible pipes. Particularly, it specifies the permissible utilization factors of bonded flexible pipe layer. The API 17 K standard

requires an accurate determination of the load response in the hose wall. But sufficient design details about theoretical calculations or numerical simulations are not available in these guidelines. The ultimate bearing capacity analysis of single carcass floating hose under internal pressure and tension loads is few in published literature. Some researchers have carried out significant work on the structural behavior of marine hoses. Vinnem et al. [5] reported several large oil spills on the Norwegian Continental Shelf due to loading hose rupture. This fact implied the importance of safety and reliability of hose.

There is limited literature about analysis of stiffened composite rubber hose under internal pressure. Zhou et al. [6] theoretically analyzed the stresses of stiffened composite rubber hose under internal pressure less than 3.0 MPa, using orthotropic elasticity method. But the influence of stiffeners on hose response is not considered. Tonatto et al. [7] conducted burst test for double carcass offloading hose to validate the two-dimensional axisymmetric finite element models. The models consider plane stress state, whereas three stress components are neglected. Gonzalez et al. [8] proposed a numerical and an analytical model to calculate the stresses and strains in each component under 1.0 MPa internal pressure. But the steel helix was reduced to a spatial beam. Other researchers conducted analysis on unstiffened composite hose and pipelines subjected to internal pressure. Based on anisotropic elastic theory, Gu et al. [9] presented the analytic solutions of stresses and elastic deformations of steel wire wound reinforced rubber hose under internal pressure. The theory cannot consider nonlinear material properties. Zheng et al. [10] and Bai et al. [12] conducted theoretical and experimental investigation on short-term burst of plastic pipes reinforced by cross helically wound steel wires or thermoplastic pipe reinforced by aramid fibers. The experimental results of Bai [12] are used in this paper for validation of finite element model.

Some research work focused on other mechanical behavior of composite hose, such as fatigue durability, crush and torsion. Lassen et al. [13] carried out experimental work with respect to extreme load resistance and fatigue durability analyses on bonded steel reinforced rubber loading hoses. The findings are referable for hose engineers. Lassen et al. [14] presented extreme load capacity assessments and a fatigue life prediction methodology for bonded rubber loading hoses, subjected to repeated reeling. Tonatto et al. [16] implemented failure and damage analyses numerically and experimentally to predict crush behavior of the hose section. Gao et al. [17] numerically calculated the stresses and strains of hose and material utilization factors under torsion.



Fig. 3. Rubberized cord fabric wound on mandrel.



Fig. 4. Steel stiffener wound on the hose.

The mechanical response of hose under internal pressure is a fundamental problem. It involves the integrity and safety of hose in oil transportation and concerns environmental protection. Besides, determination of hose burst pressure is necessary for manufacturers to ascertain the extent to which the hose can be loaded over recommended service conditions.

In this work, considering three dimensional stress state, a detailed nonlinear finite element model is created for the single carcass composite hose to predict its structural behavior under internal pressure. The rubber and cords are dealt with hyperelastic constitutive models. Interactions between steel helix, reinforcement layers and rubber are treated with embedded element technique. Large deformations of various components are considered. Strains, stresses, radial and axial deformation and load in reinforcement plies are obtained. Burst pressure and failure modes are recognized. The burst pressure can be predicted by identifying the pressure at which the cord breaking force or ultimate strength of steel stiffener is attained. The influence of different fibers and rubbers on hose pressure-deformation response are evaluated. The results demonstrate good accordance with the burst pressure requirement of the OCIMF 2009 [3]. The finite element model is validated by two experimental cases and can be a predictive tool for failure pressure of single carcass hose.

2. Validation of numerical method

Three experimental cases are adopted to validate the finite element model (FEM), which is elaborated in Section 3. Firstly, to validate the rebar approach, the pressurization experimental results of aramid fiber reinforced thermoplastic pipe by Bai et al. [12] are used for comparison with FEM results. Material and geometric properties of the pipe are based on Ref. [12]. The length of the model and boundary conditions are equal to that of the specimens in burst test. The internal pressure varies from 0 to 3.5 MPa. The axial and hoop strain of the midpoint are achieved on the pipe central section [12]. The comparison in Fig. 5 indicates that there is a good agreement between results of experiment and FEM. The rebar approach is effective to study the mechanical behavior of fiber reinforced pipe.

Secondly, according to OCIMF 2009 [3], the elongation is defined as

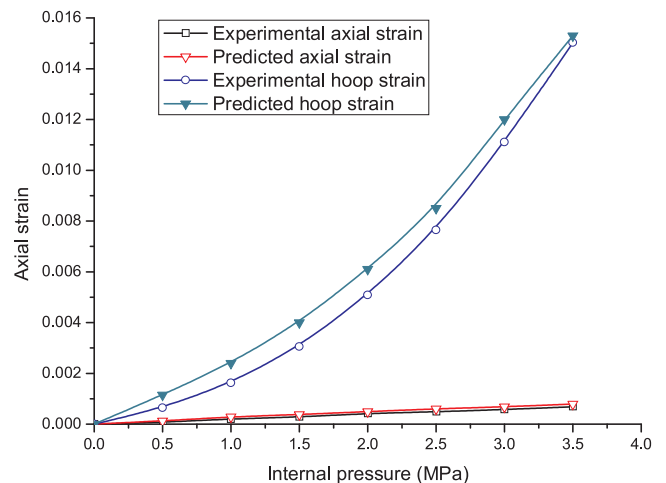


Fig. 5. Comparison of experimental strains [12] and predicted strains by FEM.

the ratio of axial displacement ΔL and sample length L . The axial stiffness $\bar{EA} = TL/\Delta L$, where T is axial tension. The variation of axial tension with elongation is almost linear, as shown in Fig. 6. The slope of tension-elongation curve means the axial stiffness. The axial stiffness by the manufacturer's test is 12.0 MN, while the prediction of FEM is 9.14 MN, a difference of 23.8% between them. The latter is slightly smaller, because the ring model assumption does not consider the axial tensile stiffness of the steel helix. The simplification of model is reasonable.

Lastly, a pressurization burst test for composite tanker rail hose is conducted, as shown in Fig. 7. The construction of the carcass of tanker rail hose is identical with mainline hose. So it is practicable to be used for model validation. The length of sample in test is 9.15 m, nominal burst pressure 7.5 MPa, the bore diameter 500 mm. As shown in the setup diagram Fig. 7(a), the hose is settled on several roller pipes for free axial movement under internal pressure. Two flanges are bolted with end caps, one end cap having a water inlet. Water pump is used to pressurize the hose and the water pressure is displayed by pressure

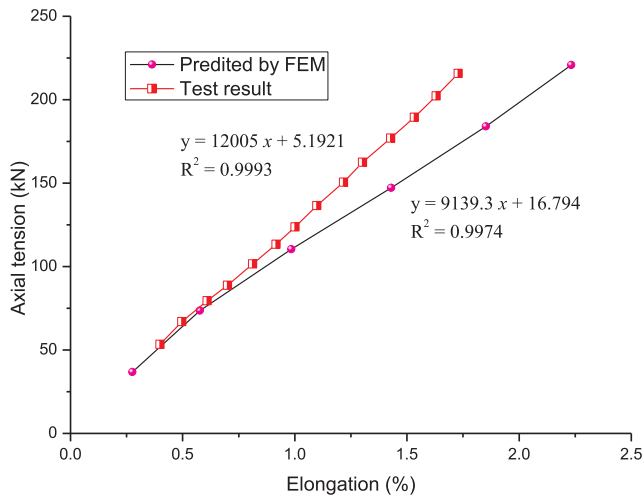


Fig. 6. Axial tensile behavior of test [15] and FEM for composite hose.

gauge in real time. Fig. 7(b) shows the bursting process of the hose in extremely short time less than a second. The hose wall ruptures close to the middle section at half hose length and then water squirts. The crack lies nearly normal to the cord direction. Cords within the crack are fractured and rubber is torn open. The stiffeners are intact. The hose failure depends on the tensile strength of cord of average 200 N. Cords firstly fail prior to stiffener. From Fig. 7(b), it can be found that the hose elongates as the internal pressure increases. When approaching failure, the hose shrinks axially. The burst pressure is 7.7 MPa, recorded by a

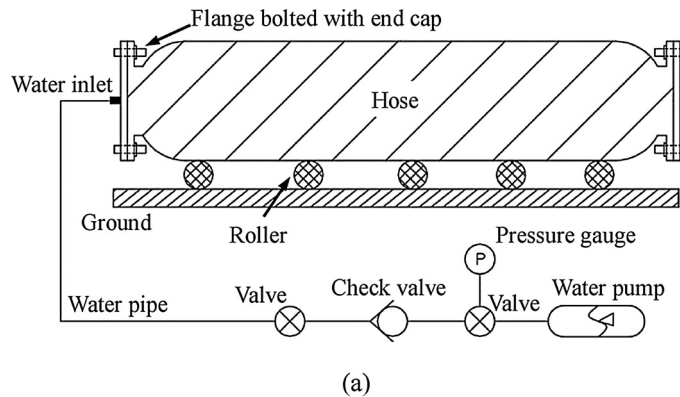
water manometer. While the FEM result of burst pressure is 9.14, a deviation of 18.7% with test. There are possibly some manufacturing defects existing in hose specimen, such as deficient interlayer bonding, bubble and delamination during rubber vulcanization, slight ovalisation of steel helix during cool-bend process. These defects could cause the decrease of burst capacity of tested specimens.

3. Finite element modeling

Finite element modelling provides a cost-effective means than prototype tests in structural analysis of hose. A three dimensional nonlinear finite element model is developed by commercial software ABAQUS /Standard (version 6.13) [19]. To get a better grasp of hose performance, the geometric and material nonlinearities are considered. General static analysis step in ABAQUS/Standard is used for the non-linear problem.

3.1. Simplification of hose model

Some proper simplifications are made for FEM in view of computational expense. The exterior rubber and underlying floatation jacket made of foam material almost contribute none for hose strength, and thus are neglected. This paper focuses on the structural behavior and burst capacity of the hose body. There is possibility that hose ruptures at central part instead of vicinity of end fitting under internal pressure. Some researchers have reported such cases for composite hose [7] or reinforced plastic pipes [10,11]. The hose body excluding end fittings is selected and modelled in finite element analysis, as shown in Fig. 8. The spacing between two stiffeners is 50 mm. A 3D quarter model with



(a)



(b)

Fig. 7. Setup diagram of burst test (a), and prototype burst test of 500 mm diameter hose (b).

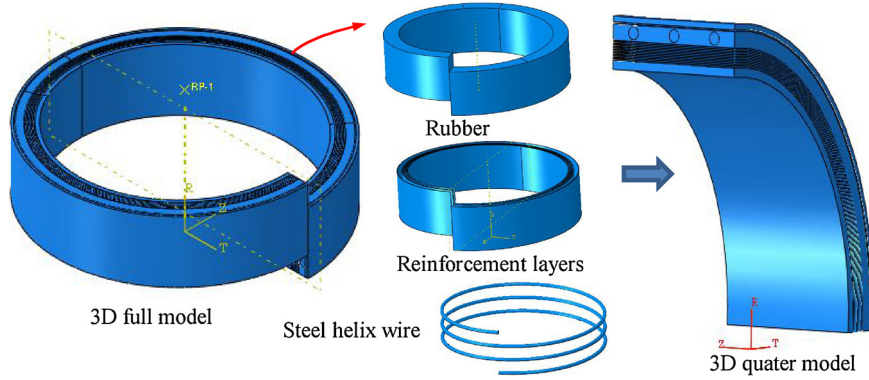


Fig. 8. Simplified hose model.

length of 150 mm is created including three spacings. The modelling methodology of composite hose refers to the work of other researchers in modelling flexible pipes [18,20–23]. The steel helix is modelled as a three-dimensional entity instead of a curved beam, considering all six stress components (normal stresses and shear stresses) used in von-Mises criterion.

Rebar (reinforcement bars) approach [19] is used to define the layer of uniaxial reinforcement in surface element. Such layer is treated as a smeared layer with a constant thickness equal to the area of each reinforcing bar divided by the reinforcing bar spacing. The following data are necessary for modelling hose behavior using the rebar approach: cords spacing (space between centers of two consecutive cords), cords cross-sectional area, cord material property, cords orientation inside a ply, number of cord plies.

3.2. Hyperelastic constitutive models for rubbers

The viscosity of rubber is not considered and is assumed to be purely hyperelastic, as done by Kondé [24]. Rubber material is isotropic and nearly incompressible. To check the influence of rubber properties on hose structural behavior, three different rubbers of various compounds are selected and fitted with respective constitutive model. In what follows, the stress-strain curves are given within strain range of 250%, as shown in Fig. 10.

(1) Ogden model

For Ogden model [25], the strain energy density function is presented as following:

$$W = \sum_{i=1}^N \frac{2\mu_i}{\alpha_i} (\bar{\lambda}_1^{\alpha_i} + \bar{\lambda}_2^{\alpha_i} + \bar{\lambda}_3^{\alpha_i} - 3) + \sum_{i=1}^N \frac{1}{D_i} (J_{el} - 1)^2 \quad (1)$$

where N determines the number of terms in the strain energy density function; the constants μ_i and α_i describe the material's shear behavior; $\bar{\lambda}_i = J^{-1/3} \lambda_i$ and λ_i denote the principal stretch ratios; $J = \lambda_1 \lambda_2 \lambda_3$ is the Jacobean determinant; J_{el} is the volume ratio, set equal to 1.0 for incompressible materials; D_i introduces compressibility and is close to zero for nearly incompressible materials. Uniaxial tensile tests are conducted with dumbbell rubber samples according to ASTM D412 [26], as shown in Fig. 9(a). The stress-strain curves are achieved to identify the parameters of the Ogden model, $\mu_1 = -2.753$ MPa, $\mu_2 = 0.199$ MPa, $\mu_3 = 2.584$ MPa, $\alpha_1 = -2.226$, $\alpha_2 = 1.334$, $\alpha_3 = -3.115$.

(2) Yeoh model

For Yeoh model [27], the strain energy density function is offered as below:

$$W = \sum_{i=1}^3 C_{i0} (\bar{I}_1 - 3)^i + \sum_{i=1}^3 \frac{1}{D_i} (J_{el} - 1)^{2i} \quad (2)$$

where \bar{I}_1 is the first invariant of the deviatoric strain tensor; C_{i0} are material constants, describing the shear behavior for the material.

Fitting the stress-strain curve, the parameters are obtained, $C_{10} = 0.9953$ MPa, $C_{20} = -0.2123$ MPa, $C_{30} = 0.0289$ MPa.

(3) Arruda-Boyce model

For Arruda-Boyce model [25], the strain energy density function is given by:

$$W = \mu \sum_{i=1}^5 \frac{C_i}{\lambda_m^{2i-2}} (\bar{I}_1 - 3)^i + \frac{1}{D} \left[\frac{J_{el}^2 - 1}{2} - \ln(J_{el}) \right] \quad (3)$$

with the material constants $C_1 = 1/2$, $C_2 = 1/20$, $C_3 = 11/1050$, $C_4 = 19/7000$, $C_5 = 519/673750$. μ is the initial shear modulus; λ_m is the locking stretch at which the upturn of the stress-strain curve would rise significantly; D is set to zero for incompressible materials. The stress-strain curve refers to Ref. [28], input into ABAQUS to fit the material parameters, $\mu = 1.114$ MPa, $\lambda_m = 1.569$, $D = 0.001$.

3.3. Cord and stiffener material models

In this work, three different polymer cords are used for comparison, i.e. polyester (PET) of linear density 3000 denier (labeled as PET-a), polyester of linear density 2000–9000 denier (labeled as PET-b) and polyamide of linear density 10,000–20,000 denier (labeled as Nylon), respectively. The material properties of cords are listed in Table 3. Uniaxial tensile tests for PET-a cord are conducted according to ASTM D885 [29], as shown in Fig. 9(b). The material properties of PET-b and Nylon cords refers to the work of Ref. [7]. The stress-strain curves are shown in Fig. 11.

The stress-strain relations for hyperelastic polymer cords are represented by Marlow's formulation [30]. Marlow's model is a general first-invariant constitutive model for incompressible, hyperelastic materials. It can replicate the stress-strain behavior of fibers once it is calibrated by uniaxial test data. The strain energy density of Marlow's model is the integral of uniaxial tensile stress $T(\epsilon)$ and the uniaxial strain $\epsilon = \lambda_T(\hat{I}) - 1$, where λ_T is the uniaxial tensile stretch, \hat{I} the first invariant. The uniaxial tensile stretch λ_T satisfies the equation

$$\lambda_T(\hat{I})^3 - \hat{I} \lambda_T(\hat{I}) + 2 = 0 \quad (4)$$

Since \hat{I} is arbitrary, assuming $U(3) = 0$, the strain energy density is given by

$$U(I) = \int_0^{\lambda_T(\hat{I})-1} T(\epsilon) d\epsilon. \quad (5)$$

Fig. 11 shows a good accordance of Marlow's model to uniaxial tensile test data for fibers. The material properties of cords are listed in Table 2.

Lassen et al. [14] state that the steel helix gives radial stiffness to the hose cross-section in order to avoid collapse when the hose is subjected to high tension or excessive external pressure. The helix steel has a SMYS (Specified Minimum Yield Stress) in the range of 600–700 MPa depending on the helix diameter. The stiffeners are made of high

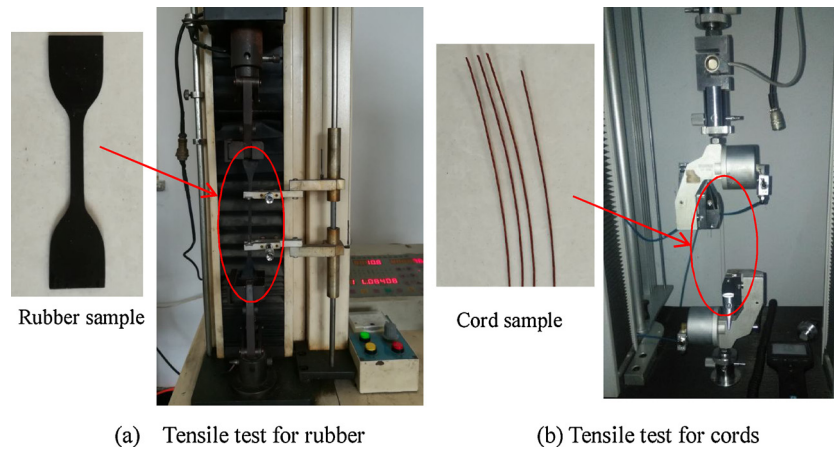


Fig. 9. Tensile test setup for rubber and cords.

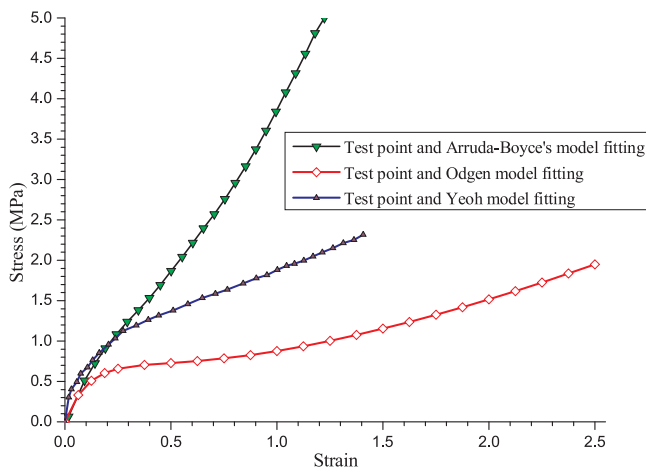


Fig. 10. Stress-strain curves of different rubbers and respective model fitting.

Table 2
Material properties of cords.

Cords	Tensile strength F_u (N)	Cross section area of cord A (mm^2)	Spacing between two cords S (mm)	Elongation at break ϵ_u (%)
PET-a	636.3 ± 5.4	0.95	1.82	19.95 ± 0.6
PET-b	200.9 ± 4.1	1.01	1.2	12.7 ± 0.4
Nylon	501 ± 12.8	3.04	1.9	24.5 ± 0.7

Table 3
Mesh details.

Components	Element type	No. of elements	No. of nodes
Rubber	C3D8RH	41,976	47,294
Reinforcements	SFM3D4	27,546	28,832
Steel stiffener	C3D8R	15,048	18,975
Total No.	–	84,480	95,101

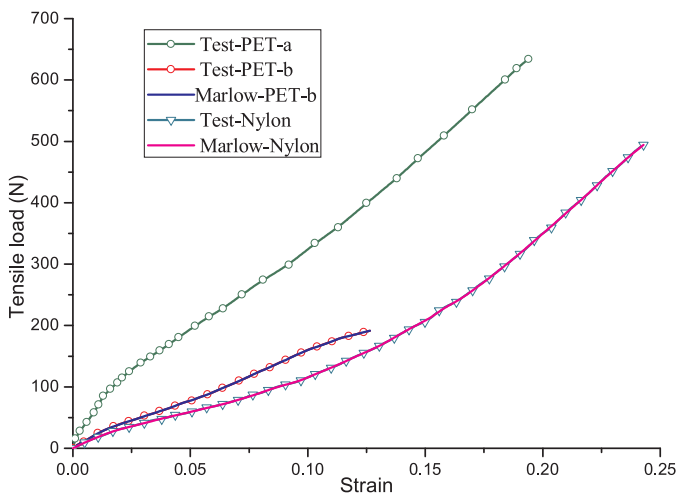


Fig. 11. Load-strain curves of hyper-elastic fibers.

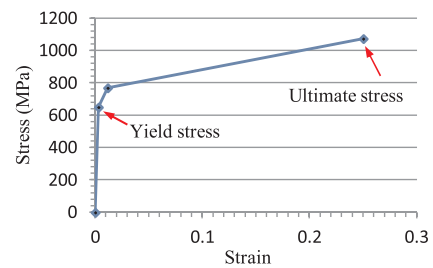


Fig. 12. Stress-strain curve of the stiffener [31].

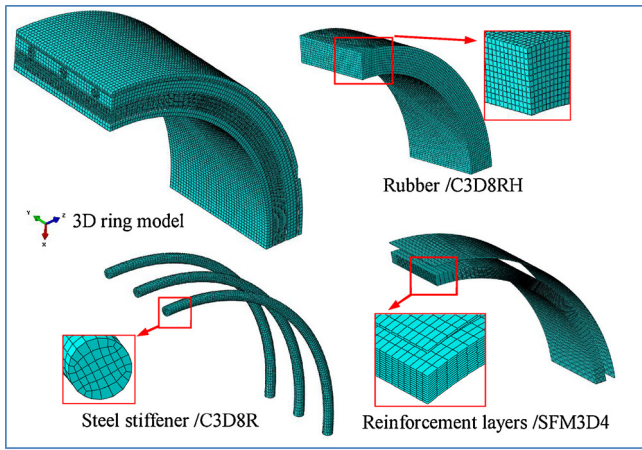
$$\sigma_e = \frac{1}{\sqrt{2}} [(\sigma_1 - \sigma_2)^2 + (\sigma_1 - \sigma_3)^2 + (\sigma_2 - \sigma_3)^2]^{1/2} < \sigma_u \tag{6}$$

where $\sigma_1, \sigma_2, \sigma_3$ are the principal normal stresses which are ordered as $\sigma_1 \geq \sigma_2 \geq \sigma_3$.

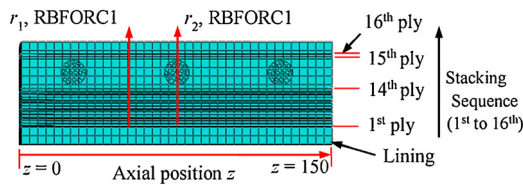
3.4. Mesh, interaction, loads and boundary conditions

The (Fig. 13) mesh details of various hose components are listed in Table 3. A mesh refinement analysis is performed to ensure result convergence of according to element size. The number of total elements of the analyzed model is 84,480. The rubber is meshed with three-dimensional continuum elements with eight nodes, linear interpolation functions and hybrid formulation (C3D8RH). Quadrilateral surface elements with four nodes (SFM3D4) are used for reinforcement plies. Linear hexahedral elements (C3D8R) with 8 nodes and reduced integration are applied to the steel stiffener. Mesh details of structural

strength carbon steel with elastoplastic behavior, as shown Fig. 12. The Young's modulus $E = 207$ GPa, Poisson's ratio $\nu = 0.3$, yield stress $\sigma_y = 650$ MPa, ultimate stress $\sigma_u = 1080$ MPa, ultimate strain $\epsilon_u = 0.25$ [31]. The von Mises yield criterion and isotropic hardening law are adopted [32]. The symbol σ_e denotes the von Mises equivalent stress for three-dimensional stress state, expressed as



(a) Mesh details of hose components



(b) Paths for result output

Fig. 13. Mesh details of hose components and paths for result output.

components are shown in Fig. 13(a). The steel stiffener and two reinforcement layers are embedded in rubber. Fig. 14(a)–(b) show the interactions of hose components.

A cylindrical coordinate system is established. A reference point (RP) is created on the hose central axis at hose end, as shown in

Fig. 14(c). It's connected with the nodes of the nearby hose end face (i.e. Region I in Fig. 14(d)) by kinematic coupling constraint, referring to the local cylindrical coordinates. All the degrees of freedom except the radial displacement are coupled. That is to say, the end face can expand radially and the longitudinal extension of the hose keeps identical with the end face. As shown in Fig. 14(d), nodes in Region III only have radial displacement. Symmetric constraints are applied to Region II in the cylindrical coordinates system. The reference point can only move axially in the global coordinate system. The internal pressure is applied to the internal surface of lining. The axial tension force is applied to the reference point which is produced by internal pressure on the closed end surface in hydrostatic test.

Trial calculation method is used to determine the hose burst pressure. The axial force $T = \pi r_0^2 P / 4$, where r_0 is the radius of hose bore, and P is internal pressure [33–35]. When internal pressure P ranges from 0.5, 1.0, 1.5, ..., 13.0, 13.5 MPa, axial force T applied to reference point varies with P . Accordingly, the loads in cords and von Mises stress are calculated and compared with materials' strength. Due to the existence of stiffeners, the radial displacement and load in cords of the composite hose will vary along axial direction. Considering the symmetry, there are two typical axial positions, one amid two stiffeners r_1 and one just below the stiffener r_2 , as shown in Fig. 13(b). Radial displacement of lining and load in cords (rebar force, RBFOR) at r_1 and r_2 are obtained.

3.5. Failure criteria

For rubberized cord fabric, the maximum stress failure criterion is employed. The cords are in state of tensile stresses under internal pressure. The material is said to have failed if one or more of the following inequalities is not satisfied [36]:

$$\sigma_1 < X_t, \sigma_2 < Y_t, |\tau_{12}| < S \quad (7)$$

where σ_1 and σ_2 are the stresses in the longitudinal and transverse fiber

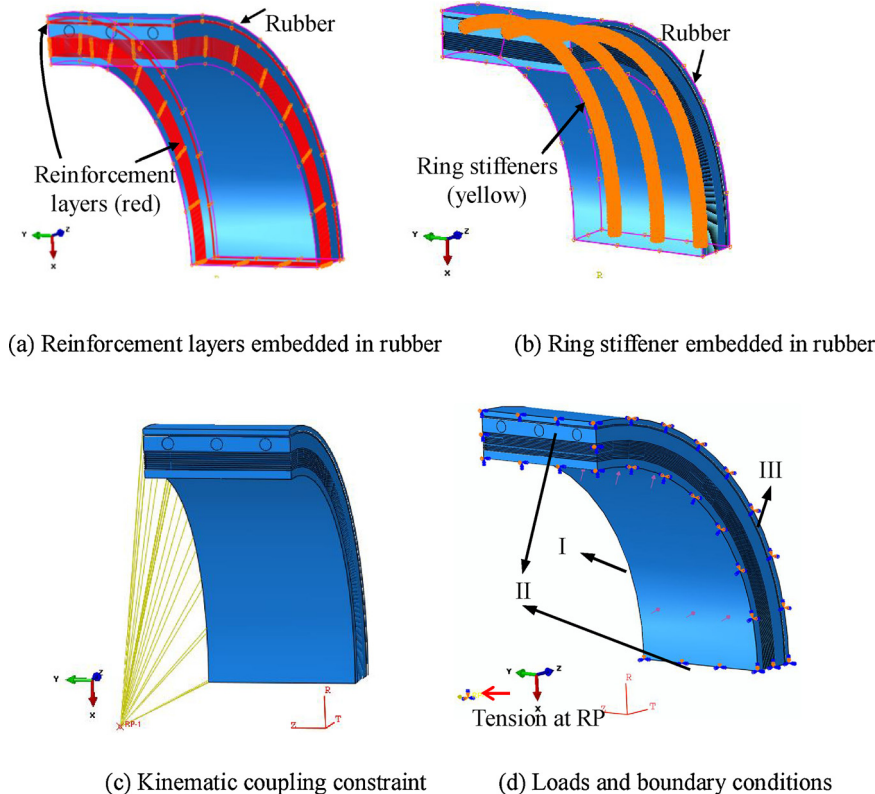


Fig. 14. Interaction, loads and boundary conditions.

directions respectively and τ_{12} is the in-plane shear stress. X_t , Y_t and S are the longitudinal and transverse tensile strengths, and the in-plane shear strength. The ultimate strain of rubber exceeds 250% in this paper, much larger than those of cords and steel. Provided the interfaces between cords and rubber are perfectly bonded, the strain of cords and rubber in the cord winding direction can be considered to be equal. When the hose is subjected to internal pressure, cords firstly reach strength limits and rupture, incurring that the hose loses the reinforcement of cords and bursts in short time. The interfacial shear failure can be neglected in burst analysis. The latter two inequalities of Eq. (7) are assumed to be satisfied readily for cord reinforced rubber structure, like hose [7] and tire [37]. Therefore, the failure pressure is obtained by monitoring σ_1 when load in cords (unit: N) reaches the cord tensile strength F_u (unit: N).

In hose design, according to standard API 17 K, the von Mises stress of steel stiffener is not allowed to exceed the yield stress under operational loads. In burst capacity analysis of hose, it is necessary to consider the plastic deformation of steel stiffener after yield to determine the final internal pressure. It is assumed that the hose fails if the von Mises stress σ_e of stiffener exceeds the ultimate strength σ_u , as Behroozi et al. [38] did for steel cords in tire under inflation pressure.

4. Results and discussion

The influence of cords on hose structural behavior is investigated using three combinations of Odgen rubber and three different cords, i.e. OdgenPET-a, OdgenPET-b and OdgenNylon. The influence of rubber elastomers is represented by OdgenPET-b, YeohPET-b and ABPET-b (Arruda-Boyce) with identical PET-b cord.

It is specified in OCIMF 2009 [3] that burst test pressure is five times the Rated Working Pressure (RWP) at which the hose should not have failure of any kind. Then the pressure will then be raised until the hose fails and the pressure at which it fails, as well as the mode and location of failure, will be recorded as the Burst Pressure. In this paper, RWP is 1.5 MPa, burst test pressure 7.5 MPa. Both are specified by purchaser and accord with requirement of OCIMF 2009. Thus the burst test pressure is a critical load to verify the hose design. The force in rebar (RBFOR) are the loads in cords and are calculated under internal pressure $P = 7.5$ MPa and axial tension $T = \pi r_0^2 P / 4 = 36.8$ kN. The numerical results are summarized in Table 4.

4.1. Load in cords

As a representative, the loads in cords (rebar force, RBFOR) of PET-a embedded in Odgen rubber under internal pressure of 7.5 MPa are shown in Fig. 15. It is notable that the stiffener changes the load distribution in cords due to its confine effect. The loads in cords are

heterogeneous. The load in cords below stiffener (Region 2) is much more concentrated than that of Region 1 between two ring stiffeners, as shown in Fig. 15(a). The maximum load in cords does not occur just below the stiffener, but occurs in the 14th layer in Region Mid, see Fig. 15(b). As shown in Fig. 16, the load distribution of cords of first reinforcement ply is spatially periodic along with axial position, which is caused by the presence of ring stiffeners. The rebar force below the stiffener is higher than the Region 1. Besides, the rebar forces increase with internal pressure.

As the internal pressure grows, redistribution of load in cords occurs, because the von Mises stresses of ring stiffener raise to the elastic limit (650 MPa) and enter the plastic hardening stage. The confine effect of stiffeners gradually diminishes. As a consequence, the axial tensile force is basically borne by reinforcement plies. The maximum load in cords transfers to the innermost reinforcement plies for OdgenPET-a hose, as shown in Fig. 17(a). The interior reinforcement plies will break after the stiffener ruptures. It is stiffener-dominated failure mode. Whereas Fig. 17(b) shows a different failure mode, that is, the cords around stiffener fail first for OdgenPET-b hose at failure pressure of 9.55 MPa.

Fig. 18 shows the load in different reinforcement plies of various radial positions, i.e. distances to the central axis of the hose, under internal pressure of 7.5 MPa. For three hose configurations of Odgen rubber and various cords, the variation curves of rebar force in are quite similar, respectively in Region below and Region Mid. For OdgenPET-a, OdgenNylon and OdgenPET-b, the maximum load is 224.5 N, 214 N and 149.2 N, respectively, occurring in the 14th plies between ring stiffeners. The maximum load of reinforcement plies below the coil present in the 12th plies and is 224.2 N, 163 N and 137 N, respectively. The material utilization factors of PET-a, nylon and PET-b which equals load divided by ultimate tensile strength are 0.353, 0.427 and 0.743. The material utilization factor is one of the design criteria specified by API 17 K. It is demonstrated that all the three hose configurations are able to bear the burst test pressure (7.5 MPa) and axial force due to closed-end effect.

Fig. 19 shows the influence of rubber properties on the rebar force, taking fiber PET-b for example. For OdgenPET-b, the maximum load is 149.2 N in 14th ply between ring stiffeners. For YeohPET-b and ABPET-b, the maximum load is 182.7 N and 155 N, respectively, occurring in the 12th plies below the stiffener. The material utilization factors in turn are 0.743, 0.772 and 0.909. They are not beyond the permissible utilization factor 0.91 as specified in API 17 K. Considering potential manufacturing deficiency, the ABPET-b hose configuration is not recommended.

A redistribution of the cord load occurs at a radial position close to 275 mm from the hose center in Figs. 18 and 19. For rebar force in Region 2 (RBFOR2), it is caused by the stiffener and its circumambient

Table 4
Calculations for various hose configurations.

Rubber/cords	Failure mode	Failure pressure (MPa)	Internal pressure (MPa)	r_1 (mm)	r_2 (mm)	Axial elongation (%)	Stress of stiffener (MPa)
Odgen/PET-a	Stiffener fails.	13.50	1.5	0.8	0.5	0.27	85.4
			7.5	4.5	3.5	2.17	535.3
			13.50	75.1	74.8	-0.94	1021.4
Odgen/Nylon	Stiffener fails.	10.40	1.5	2.4	1.7	1.19	113.6
			7.5	9.2	7.4	5.00	707.3
			10.40	83.6	82.9	0.44	1039.0
Odgen/PET-b	Cords break.	11.05	1.5	1.3	0.9	0.54	102.2
			7.5	6.0	4.8	3.17	655.6
			11.05	53.2	52.5	1.04	933.4
Yeoh /PET-b	Cords break.	9.55	1.5	1.50	1.11	0.58	109.7
			7.5	7.2	6.0	3.42	672.8
			9.55	17.8	16.7	18.5	804.1
AB /PET-b	Cords break.	9.14	1.5	1.54	1.13	2.95	101.0
			7.5	7.1	5.8	17.95	662.9
			9.14	10.4	9.1	20.2	769.9

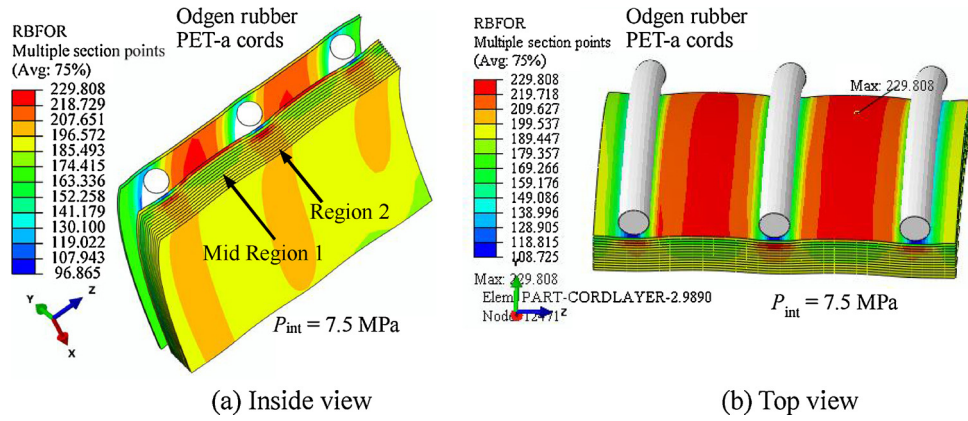


Fig. 15. Load in cords for OdgenPET-a hose.

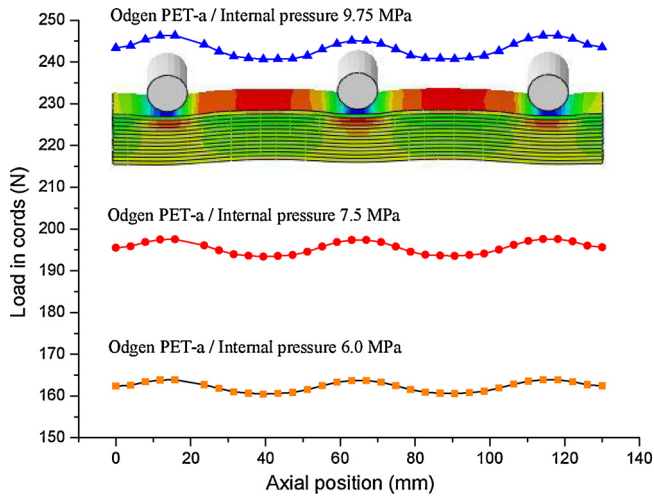


Fig. 16. Load in cords of 1st ply in OdgenPET-a hose with internal pressure.

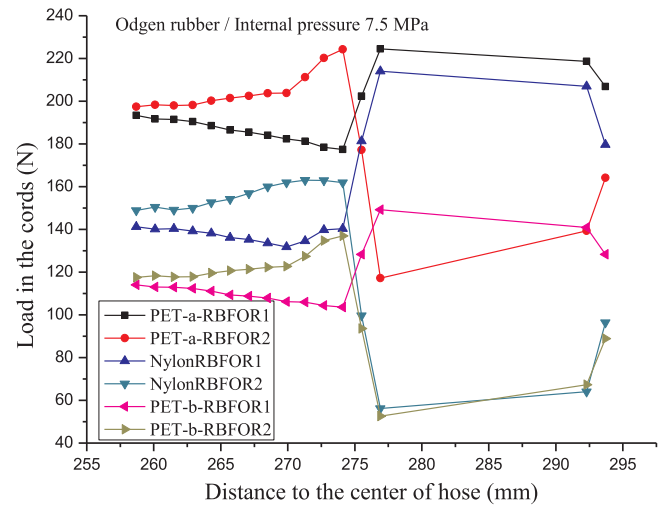


Fig. 18. Influence of cords properties on load in cords.

filling rubber. From Fig. 15(a), Figs. 18 and 19, it can be found that the cord loads in 13th and 14th ply below the stiffener are smaller than those in 1st to 12th ply, and at the same level with 15th and 16th ply above the stiffener. It is justified by the fact that the stiffener is bonded with its near cord plies by circumambient filling rubber and restricts the deformation of cords. Additionally, the filling rubber between stiffener and cord plies acts as a pillow for cords and reduces the bending curvature caused by internal pressure. For rebar force in Region 1 (RBFOR1) amid two stiffeners, the cord loads in 13th and 14th ply are larger than those 1st to 12th ply, because the bending by pressure push and stretch added by filling rubber. In a word, the stiffener and filling

rubber jointly affect the loads in cords of near plies, compared with those plies away from stiffener.

4.2. Stress of ring stiffener

As observed in Fig. 20, the steel ring stiffener response with internal pressure is basically linear up to the limit of elasticity, namely the yielding strength 650 MPa. Beyond this point, the stiffener presents a plastic hardening state. For OdgenPET-a, OdgenNylon and OdgenPET-b, the maximum von Mises stress of stiffener is 1021.4 MPa, 1039 MPa, and 933.4 MPa, respectively. In the former two hose configurations, the

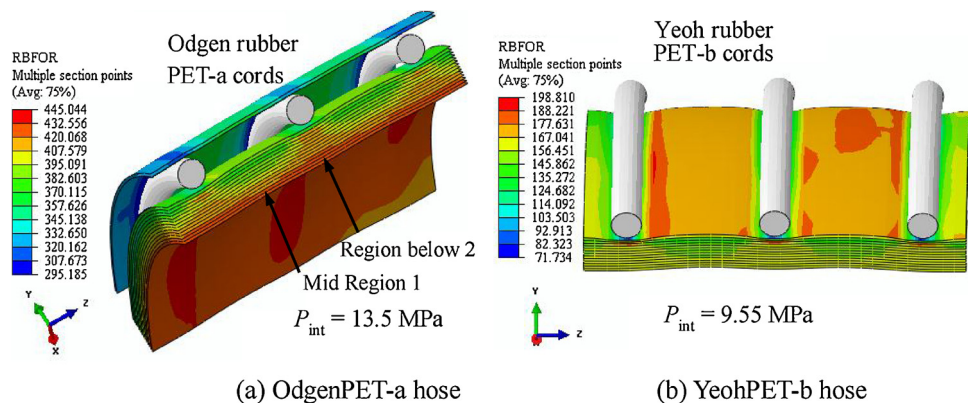


Fig. 17. Load in cords at failure pressure.

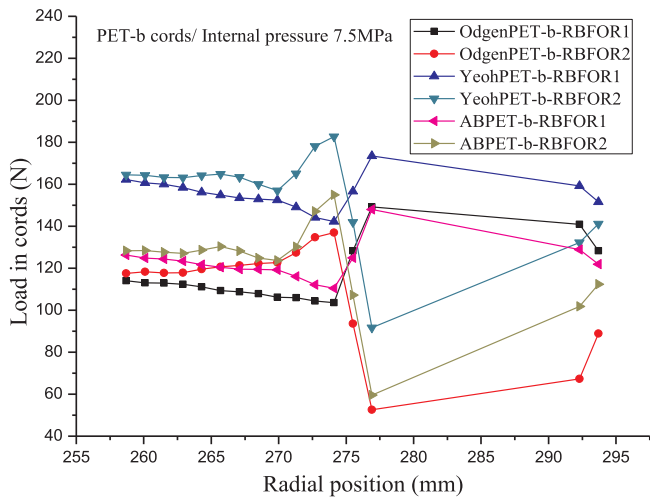


Fig. 19. Influence of rubber properties on load in cords.

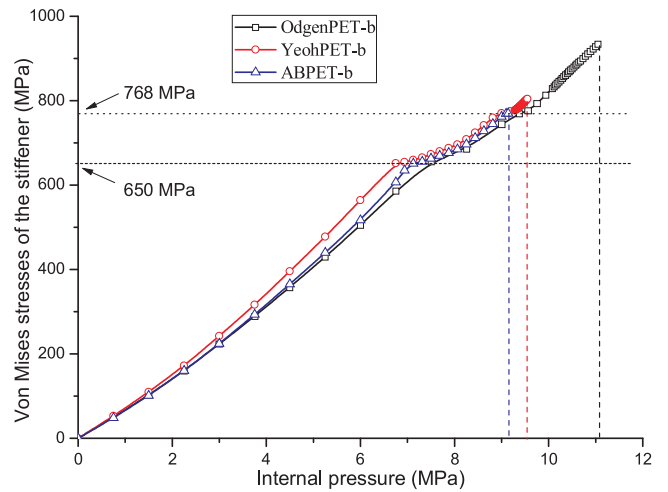


Fig. 21. Influence of rubber on stresses of stiffener.

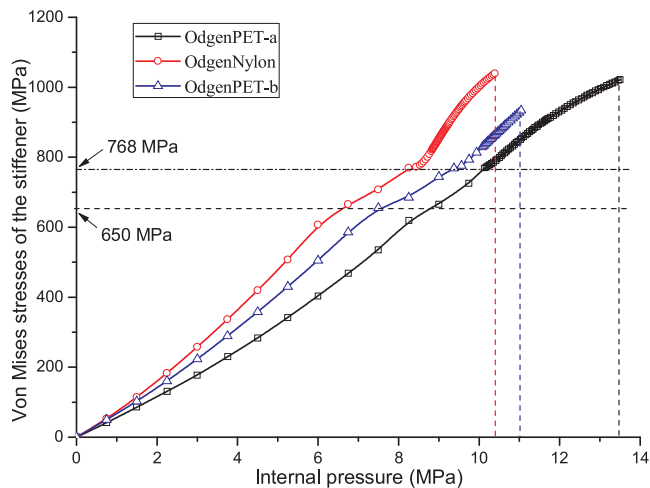


Fig. 20. Influence of cords on stresses of stiffener.

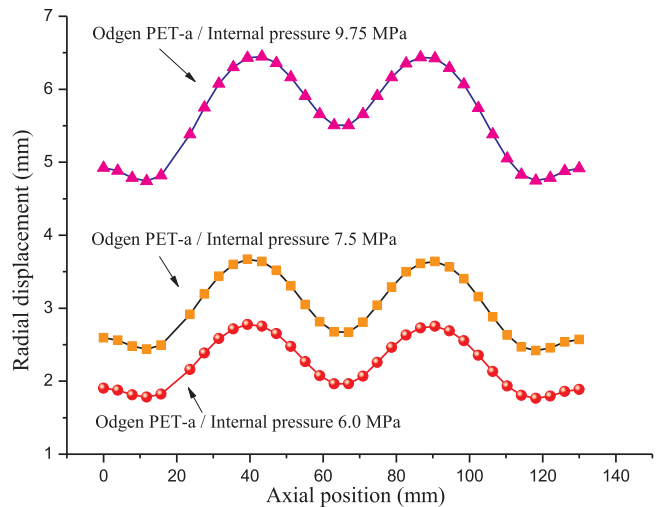


Fig. 22. Radial displacement of lining under various internal pressures.

steel stiffeners firstly reach the ultimate tensile strength prior to the rupture of cords. For the third hose configuration, the cords will break at internal pressure 11.05 MPa before stiffener fails. The slopes of stresses-pressure curves vary with internal pressure due to the three-piece constitutive curve of carbon steel. The stiffener of OdgenNylon hose firstly yield at about 6.5 MPa and the von Mises stresses ascend rapidly in the second plastic hardening stage. The stiffener of OdgenPET-b hose has just yielded at pressure of 7.5 MPa, while the stiffener of OdgenPET-a hose still stays elastic. This is justified by the fact that the secant modulus of nylon cords is smaller compared with polyester cords in the strain range within 0.15. The cord properties have crucial effect on the stress evolution of stiffener with internal pressure.

As shown in Fig. 21, the different constitutive models of rubber have relatively little effect on the stresses of stiffener than fiber cords. For OdgenPET-b, YeohPET-b and ABPET-b, when cords break, the stress of stiffener is 933 MPa, 804 MPa and 770 MPa, far from ultimate tensile strength. Correspondingly, the burst pressure of the above hose configurations is 11.04 MPa, 9.55 MPa and 9.14 MPa. The internal pressures under which the stiffeners begin to yield are very close, near about 7.3 MPa. The last two configurations have nearly the same burst pressure, because of their similar stress-strain curves of rubber within strain range of 0.25.

4.3. Radial displacement

As shown in Fig. 22, for OdgenPET-a hose, the radial displacement curve of the node of lining increases with internal pressure. The trends of three curves indicate a bulging effect of the reinforced rubber. The internal pressure pushes the lining and reinforcement layers against the stiffener, and results in the bending of reinforcement layers and lining. The bending causes a small curvature of rubber lining. The maximum radial displacement is 3.64 mm under burst test pressure of 7.5 MPa. Figs. 23 and 24 shows the influence of cords and rubber properties on radial displacement, compared with Ref [7]. by two dimensional axisymmetric simulations. The variation trends agree well till the failure pressure. The upturn points of curves mean the yielding of stiffener. They are at similar level of radial displacement due to the close yield strength of steel stiffener. The yield stress in this paper is 650 MPa, little smaller than 725 MPa in Ref. [7]. Thus the upturn points of pressure-displacement curves of hoses in this paper arise at lower internal pressure. After yielding of steel stiffener, there is a quick increase of the curve due to the good plasticity of stiffener.

Fig. 23 shows that the radial displacements of lining rubber between and below stiffeners, i.e. r_1 and r_2 , increase with internal pressure in the beginning. And the deviation between r_1 and r_2 grows. Besides, as the stiffener yields and turns into plastic hardening state, the difference decreases and almost coincides in the second plastic stage. It is testified by the upturns on the displacement curves. For OdgenPET-a hose and

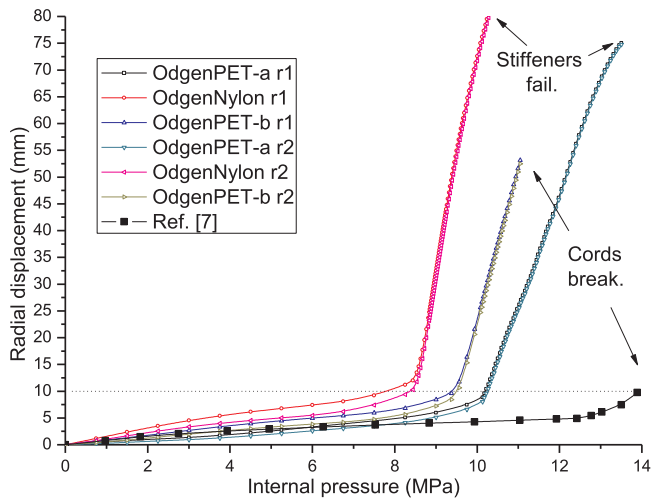


Fig. 23. Influence of cords properties on radial displacement.

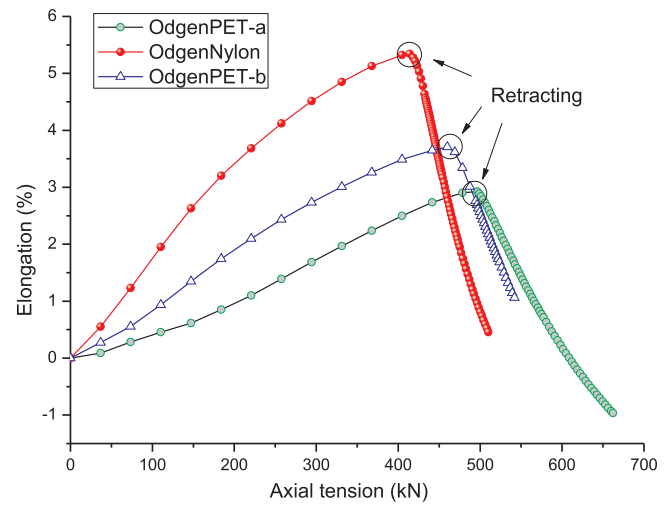


Fig. 25. Influence of cords properties on axial elongation.

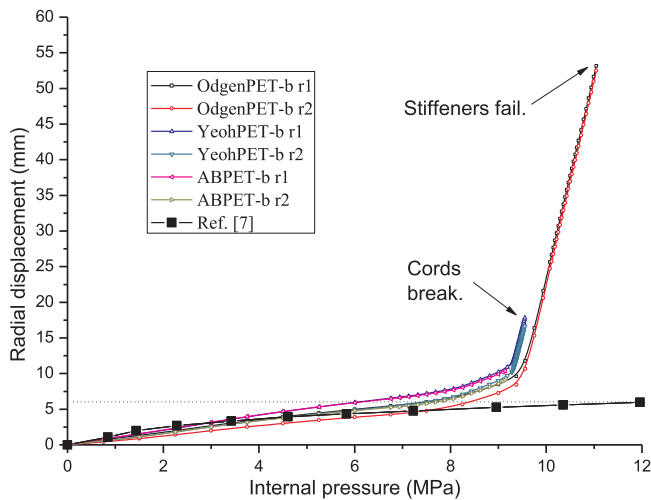


Fig. 24. Influence of rubber properties on radial displacement.

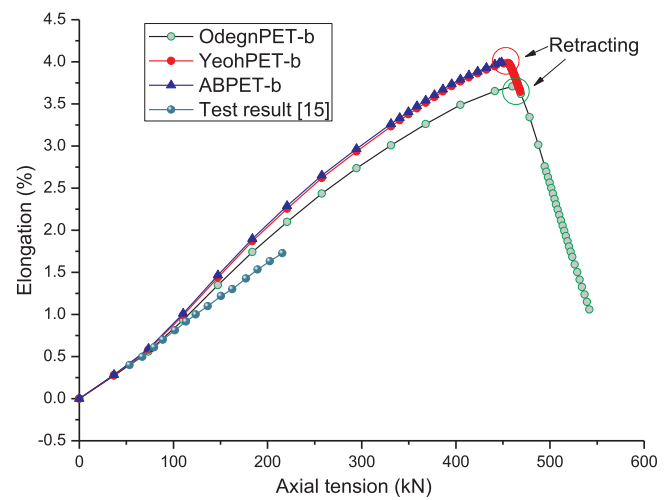


Fig. 26. Influence of rubber properties on axial elongation.

OdgenNylon hose, r_1 and r_2 exceed 70 mm when approaching stiffener failure. Because the von Mises stresses of stiffener undergo plastic hardening till the ultimate strength and reach 1021.4 MPa and 1039 MPa, respectively. For OdgenPET-b, the stiffener also enters the second plastic hardening stage till the cords rupture. By this point, the stress of stiffener is 933.4 MPa. The variation trend of radial displacement verifies the confine effect of stiffeners.

The influence of rubber material properties on radial displacement is not as apparent as that of fibers, as shown in Fig. 24. With identical fibers of PET-b, hoses of Arruda-Boyce rubber and Yeoh rubber present almost the same variation curves of radial displacement while internal pressure is within 7 MPa. From then on, the difference of r_1 displacements increases gradually as the stiffener yields. It is the same case for r_2 displacements. Finally, when the cords approach to breaking force, the r_1 and r_2 displacements for Arruda-Boyce hose are 10.4 mm, 9.1 mm, and for Yeoh rubber hose 17.8 mm and 16.7 mm, respectively. The former configuration fails prior to the latter one. It is remarkable that the Odgen rubber hose has the largest failure radial displacement. However, its von Mises stress of stiffener is 933 MPa, higher than the other two cases, and its stiffeners have larger plastic deformation. It demonstrates that rubber and stiffener work together to restrain the radial expansion.

4.4. Axial elongation

The axial tensile force due to closed-end effect produces the axial elongation of hose. Fig. 25 and 26 shows the influence of cords and rubber properties on axial elongation. The model tension-elongation behavior in this paper is verified by nondestructive tensile result in Ref. [15]. The slope of tension-elongation curve means the axial stiffness. The axial stiffness by the test is 12.0 MN, while the prediction of FEM is 9.14 MN, a difference of 23.8% between them. The latter is slightly smaller, because the ring model assumption does not consider the axial tensile stiffness of the steel helix. The retracting points on the curves demonstrate that hoses begin to become short after stiffeners yield and enters plastic deformation, meanwhile hoses expand in radial direction. The hose extension behavior is nonlinear due to the hyperelastic material properties of rubber and cords, as shown in Fig. 25. The hose with nylon cords presents the largest elongation before its downturn point on the curve, which indicates that the hose begins to retract axially. At this moment, the stiffener enters the second plastic hardening stage and the hose sharply expands in radial direction. This elucidates that the axial elongation relates to the plastic deformation of stiffeners. The eventual elongation for OdgenPET-a, OdgenNylon and OdgenPET-b hose is -0.94%, 0.44% mm and 1.04%, respectively. The axial elongation of the hose with PET-a cords is the smallest within internal pressure of 8.5 MPa. However, its final length becomes shorter compared with its original length.

As regards the influence of rubber material properties on hose axial elongation, it can be seen that Arruda-Boyce model and Yeoh model present nearly identical variation tendency when internal pressure is less than 9 MPa, as shown in Fig. 26. The elongation difference between Odgen model hose and Yeoh model hose increases because their stress-strain relations differ more as strain grows. The ABPET-b hose configuration does not exhibit axial shrinkage. Its maximum stiffener stress is 770 MPa, just at the start point of the second plastic hardening. In a word, rubber mainly effects the plastic stress state of stiffeners and subsequently effects the radial and axial deformation.

4.5. Failure pressure analysis

The failure pressure can be predicted by identifying the pressure at which the cord breaking force or the stiffener tensile strength is attained. The material properties of fibers and rubbers exert varying degrees of influence on the hose failure pressure. Fiber properties are more influential than rubbers. From Table 4, it can be seen that the maximum difference of failure pressure is 29.9% among the three hose configurations of Odgen rubber fitting. Though they possess the same Odgen rubber fitting, failure modes of hoses with PET-a and PET-b fibers are quite different. In the condition that stiffeners of both hoses enter plastic hardening, PET-b cord firstly reaches the breaking force. Even with higher tensile strength, nylon cords have smallest secant modulus and are easier to stretch, the failure pressure of OdgenNylon hose is minimal due to premature stiffener failure.

Regarding the effect of rubber on failure pressure, the discrepancy of failure pressure is the largest between Arruda-Boyce and Odgen rubber hose reinforced by PET-b cords, being 20.9%, because of their much different constitutive models. In general, rubber properties have certain influence on the loads in cords, stresses of stiffener and consequently bring impact on hose failure pressure. Under burst test pressure of 7.5 MPa, the results demonstrate good accordance with requirement of the OCIMF 2009 [3].

5. Conclusions

In this study, a detailed nonlinear finite element model with rebar technique is established and validated for ring-stiffened composite offshore rubber hose. The nonlinear material properties, interactions between components and large deformations are considered. The loads of cords, stresses of stiffener, radial and axial deformations of hoses with different configurations are attained. The influence of different material properties of cords and rubbers on hose mechanical performance is studied.

It is important to emphasize that stiffener imposes significant effect on hose mechanical behavior. The stiffener restricts the radial expansion of hose, leading to a bulging phenomenon of cord plies between two adjacent stiffeners under internal pressure. The presence of stiffeners also changes the distribution of loads in cords, bring about load concentration in local regions below stiffener and amid two stiffeners. Attention should be paid to these regions for structural strength check in hose design. That is the difference with common unstiffened laminated composite pipes. The failure modes and failure pressure are dependent on the joint work of cords and stiffener, i.e. cords reaches breaking force and/or steel stiffener attains ultimate tensile strength. The axial tension-elongation behavior presents slight nonlinearity due to the hyperelasticity of cords and rubber before stiffener yielding. The influence of cords properties on hose radial displacement and axial elongation is dominant compared with rubbers. Rubber mainly effects the plastic stress state of stiffeners and subsequently effects the radial and axial deformation of hose. The FE model offers a good understanding of the hose mechanical behavior and failure mechanism under internal pressure. It is important that more prototype tests are the objective of the ongoing research next.

Acknowledgements

This work is financially supported by National Key Research and Development Plan (Grant No. 2016YFC0303704) and National Natural Science Foundation of China (Grant No. 51509258).

References

- [1] OCIMF, Single Point Mooring Maintenance and Operations Guide, Oil Companies International Marine Forum, 2015.
- [2] Northcutt VM, Bonded flexible pipe, Oceans 2000 MTS/IEEE Conference and Exhibition, Providence, RI, USA; September, 2000, pp. 1407–1412.
- [3] OCIMF, Guide to Manufacturing and Purchasing Hoses for Offshore Moorings, Oil Companies International Marine Forum, 2009.
- [4] API SPEC 17K, Specification for Bonded Flexible Pipes, (2010) May.
- [5] J.E. Vinnem, B.R. Wagnild, B. Heide, New approach to risk monitoring for acute environmental spill to sea on the Norwegian continental shelf, in: SPE European health, Safety and Environmental Conference in Oil and Gas Exploration and Production, (2011), pp. 273–280 Paper No. SPE 140470.
- [6] Y. Zhou, M.L. Duan, J.M. Ma, G.M. Sun, Theoretical analysis of reinforcement layers in bonded flexible marine hose under internal pressure, Eng. Struct. 168 (2018) 384–398.
- [7] M.L.P. Tonatto, V. Tita, R.T. Araujo, M.M.C. Forte, S.C. Amico, Parametric analysis of an offloading hose under internal pressure via computational modeling, Mar. Struct. 51 (2017) 174–187.
- [8] G.M. Gonzalez, J.R.M. Sousa, L.V.S. Sagrilo, A study on the axial behavior of bonded flexible marine hoses, Mar. Syst. Ocean Technol. 11 (3–4) (2016) 31–43.
- [9] F. Gu, C. Huang, J. Zhou, L. Li, Mechanical response of steel wire wound reinforced rubber flexible pipe under internal pressure, J. Shanghai Jiaot. Univ. Sci. 14 (2009) 747–756.
- [10] J.Y. Zheng, Y.J. Gao, X. Li, X.F. Lin, et al., Investigation on short-term burst pressure of plastic pipes reinforced by cross helically wound steel wires, Zhejiang Univ. Sci. A 9 (5) (2008) 640–647.
- [11] A. Onder, O. Sayman, T. Dogan, N. Tarakcioglu, Burst failure load of composite pressure vessels, Compos. Struct. 89 (1) (2009) 159–166.
- [12] Y. Bai, F. Xu, P. Cheng, M.F. Badaruddin, M. Ashri, Burst capacity of reinforced thermoplastic pipe (RTP) under internal pressure, in: ASME 2011 30th International Conference on Ocean, Offshore and Arctic Engineering, Paper No. OMAE2011-49325.
- [13] T. Lassen, A.L. Eide, T.S. Meling, Ultimate strength and fatigue durability of steel reinforced rubber loading hoses, ASME 2010 29th International Conference on Ocean, Offshore and Arctic Engineering, (2010), pp. 277–286.
- [14] T. Lassen, A.I. Lem, G. Imingen, Load response and finite element modelling of bonded offshore loading hoses, The International Conference on Offshore Mechanics and Arctic Engineering-OMAE, (2014), pp. 8–13.
- [15] Y.J. Xu, X.L. Guo, H. Xu, Y.S. Luo, Theoretical and experimental analysis on tensile property of offshore floating oil hose, Oil & Gas Storage & Transportation 32 (2) (2013) 131–134 in Chinese.
- [16] M.L.P. Tonatto, M.M.C. Forte, V. Tita, S.C. Amico, Progressive damage modeling of spiral and ring composite structures for offloading hoses, Mater. Design 108 (2016) 374–382.
- [17] Q. Gao, Z.L. Li, D.W. Zhao, et al., Structural behavior of offshore bonded rubber hose under torsion, in: Menglan Duan, Youngsoo Yang (Eds.), Proceedings of SUCC 2016 on Subsea Engineering, Beijing, 2016, pp. 246–257.
- [18] Y. Bai, T. Liu, P. Cheng, S. Yuan, D. Yao, G. Tang, Buckling stability of steel strip reinforced thermoplastic pipe subjected to external pressure, Compos. Struct. 152 (2016) 528–537.
- [19] ABAQUS/Standard, Theory Manual and Example Problems Manual, Release 6.13 (2013).
- [20] M.G. Tang, Q.Z. Lu, J. Yan, Q.J. Yue, Buckling collapse study for the carcass layer of flexible pipes using a strain energy equivalence method, Ocean Eng. 111 (2016) 209–217.
- [21] C.P. Pesce, C.A. Martins, A.G. Neto, et al., Crushing and wet collapse of flowline carcasses: a theoretical-experimental approach, ASME 2010 29th International Conference on Ocean, Offshore and Arctic Engineering, (2010), pp. 521–529.
- [22] A.G. Neto, C.A. Martins, C.P. Pesce, C.O.C. Meirelles, E.R. Malta, et al., Prediction of burst in flexible pipes, J. Offshore Mech. Arct. Eng. 135 (2013) 011401-1-9.
- [23] A.G. Neto, C.A. Martins, Flexible pipes: influence of the pressure armor in the wet collapse resistance, J. Offshore Mech. Arct. Eng. 136 (2014) 031401-1-8.
- [24] A.K. Kondé, I. Rosu, F. Lebon, O. Brardo, B. Devésá, On the modeling of aircraft tire, Aerosp. Sci. Technol. 27 (1) (2013) 67–75.
- [25] A. Ali, M. Hosseini, B.B. Sahari, A review of constitutive models for rubber-like materials, Am. J. Eng. App. Sci. 3 (1) (2010) 232–239.
- [26] ASTM D412-16, Standard Test Methods for Vulcanized Rubber and Thermoplastic Elastomers-Tension, ASTM International, West Conshohocken, PA, 2016.
- [27] J.X. Liu, Z.P. Wang, T. Deng, FEA on steel wire braided hydraulic hose under internal pressure, China Rubber Ind. 61 (5) (2014) 300–303 in Chinese.
- [28] T.H. Zhang, W. Wang, Finite element analysis and experimental study of rubber fatigue life, China Elastomers 27 (2) (2017) 10–14 in Chinese.
- [29] ASTM D885 / D885M-10A (2014) e1, Standard Test Methods for Tire Cords, Tire Cord Fabrics, and Industrial Filament Yarns Made from Manufactured Organic-Base Fibers, ASTM International, West Conshohocken, PA, 2014.
- [30] R.S. Marlow, A general first-invariant hyperelastic constitutive model, in:

- Muhr Busfield (Ed.), Constitutive Models for Rubber III, third edition, 2003, pp. 157–160 London.
- [31] R. Cuamatzi-Melendez, O. Castillo-Hernández, A.O. Vázquez-Hernández, M. Vaz, Finite element modeling of burst failure in unbonded flexible risers, *Eng. Struct.* 87 (2015) 58–69.
- [32] C. An, M.L. Duan, R.D. Toledo Filho, S.F. Estefen, Collapse of sandwich pipes with PVA fiber reinforced cementitious composites core under external pressure, *Ocean Eng.* 82 (2014) 1–13.
- [33] M. Xia, H. Takayanagi, K. Kemmochi, Analysis of multi-layered filament-wound composite pipes under internal pressure, *Compos. Struct.* 53 (4) (2001) 483–491.
- [34] J.Z. Xing, P. Geng, T. Yang, Stress and deformation of multiple winding angle hybrid filament-wound thick cylinder under axial loading and internal and external pressure, *Compos. Struct.* 131 (2015) 868–877.
- [35] I.A. Guz, M. Menshykova, J.K. Paik, Thick-walled composite tubes for offshore applications: an example of stress and failure analysis for filament-wound multi-layered pipes, *Ships Offshore Struct.* 12 (3) (2017) 304–322.
- [36] R.M. Jones, *Mechanics of Composite Materials*, second edition, Taylor and Francis, Inc., Philadelphia, PA, 1999.
- [37] K.M. Jeong, Prediction of burst pressure of a radial truck tire using finite element analysis, *World J. Eng. Technol.* 04 (2) (2016) 228–237.
- [38] M. Behroozi, O.A. Olatunbosun, W. Ding, Finite element analysis of aircraft tyre – effect of model complexity on tyre performance characteristics, *Mater. Design* 35 (2012) 810–819.